Journal of Photochemistry & Photobiology A: Chemistry 390 (2020) 112339

Contents lists available at ScienceDirect

Journal of Photochemistry & Photobiology A: Chemistry

journal homepage: www.elsevier.com/locate/jphotochem

A novel mitochondrial targeting fluorescent probe for ratiometric imaging SO_2 derivatives in living cells

Xiao-Bo Wang[a], Hui-Jing Li[a,**], Zhenxing Chi[a], Xianshun Zeng[b,**], Li-Juan Wang[c], Yun-Fei Cheng[a], Yan-Chao Wu[a,d,*]

[a] School of Marine Science and Technology, Harbin Institute of Technology, Weihai 264209, China
[b] Tianjin Key Laboratory for Photoelectric Materials and Devices, Key Laboratory of Display Materials & Photoelectric Devices, Ministry of Education, School of Materials Science & Engineering, Tianjin University of Technology, Tianjin 300384, China
[c] School of Materials Science and Engineering, Harbin Institute of Technology, Weihai 264209, China
[d] Weihai Institute of Marine Biomedical Industrial Technology, Wendeng District, Weihai 264400, China

ARTICLE INFO

Keywords:
Pyrazoline-cyanine dye
SO_2 derivatives
Color
Emission shift
Imaging
Mitochondria

ABSTRACT

As an important endogenous signaling molecule, SO_2 plays a key role in many physiological processes. However, excessive intake of SO_2 and its derivatives lead to serious health complications of various diseases. In order to study the role of SO_2 and its derivatives in the biological environment, it is of great significance to develop new and effective monitoring methods. Here, a new red emission fluorescent probe (**TNPI**) based on pyrazoline and hemicyanine dyes for the high selective detection of SO_2 derivatives was developed. The probe **TNPI** showed some advantages such as long emission wavelength (640 nm), obvious color and fluorescence changes after reaction with SO_2 derivatives, high selectivity and sensitivity toward SO_2 derivatives (detection limit = 80 nM), and large fluorescence emission shift (160 nm) and signal ratio change (from 0.45–445, about 989 times). Intriguingly, the probe was successfully exploited for the fluorescence imaging of SO_2 derivatives in the mitochondria of living cells with low cytotoxicity.

1. Introduction

Sulfur dioxide (SO_2), a colorless, pungent and decaying odor gas, exists in the form of sulfites (SO_3^{2-}) and bisulfite (HSO_3^-) in aqueous media. Epidemiological studies have demonstrated that the excessive intake of SO_2 derivatives (SO_3^{2-} and HSO_3-) may lead to may be associated with many diseases such as respiratory system diseases, nervous system diseases and lung cancer [1–3]. It is worth noting that sulfites were classified as carcinogens by the world health organization and the international agency for research on cancer (IARC) on 27 October 2017. Despite their numerous harmful properties, SO_2 derivatives are widely involved in our daily life [4–6]. With the increasing consumption of petroleum, SO_2 are becoming as more and more serious environmental pollutants [7,8]. SO_2 derivatives can also be produced endogenously in mitochondria during the biosynthesis of thiol-containing amino acids [9–11]. Therefore, the development of highly selective and sensitive methods for the detection of SO_2 derivatives in living cells becomes a high priority.

In contrast with other methods [12–16], fluorescence detection is seen as one of the most desirable methods because of its simplicity, high sensitivity and low detection limits [17–22]. Until now, majority of the reported fluorescent probes for SO_2 derivatives are based on nucleophilic addition of SO_2 derivatives to C=C, C=N, C=O and N=N bonds. But there are still many difficulties to overcome. First, some fluorescent probes can only detect SO_2 derivatives in a single wavelength, which cannot avoid the influence of instrument and environment fluctuations [23–26]. Second, some fluorescent probes have short emission wavelengths (< 600 nm) that limit their biological applications [27–35]. Next, some ratio probes have short emission shifts and small signal emission ratio after reacting with SO_2 derivatives, which could not avoid the overlap of two emission wavelengths [36,37]. Some fluorescent probes are required to detect sulfur dioxide in a high proportion of organic solvents [38,39]. Finally, the role of SO_2 derivatives in bodies is unclear due to a lack of suitable detection methods in cells and subcellular organelles. Therefore, it is of great significance to develop an organelle targeting long wavelength emission fluorescence probe with high signal ratio for detection of SO_2 derivatives in the environment and biological systems.

* Corresponding author at: School of Marine Science and Technology, Harbin Institute of Technology, Weihai 264209, China.
** Corresponding authors.
E-mail addresses: lihuijing@iccas.ac.cn (H.-J. Li), xshzeng@tjut.edu.cn (X. Zeng), ycwu@iccas.ac.cn (Y.-C. Wu).

https://doi.org/10.1016/j.jphotochem.2019.112339
Received 28 October 2019; Received in revised form 17 December 2019; Accepted 22 December 2019
Available online 24 December 2019
1010-6030/

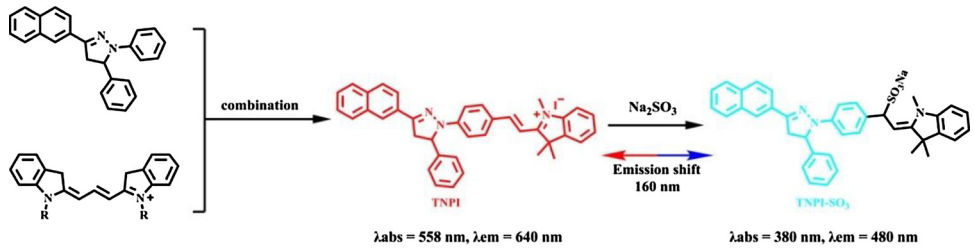

Scheme 1. Design of the Ratiometric Fluorescent Probe **TNPI** and Sensing Mechanism.

Herein, a novel mitochondrial-targeted fluorescent probe (**TNPI**) with red emission (640 nm) for monitoring SO_2 derivatives was developed in this work. In this probe, the hemicyanine moiety was selected because it can be used as an extended conjugated group and an identification group of the SO_2 derivatives. The probe **TNPI** has some advantages shown as follows: (1) a long emission wavelength (640 nm); (2) a ratio of two channels to detect SO_2 derivatives; (3) large emission shift (160 nm); (4) remarkable limit of detection (80 nM); (5) up to 989-fold signal ratio enhancement (from 0.45–445). Moreover, to demonstrate its potential practical applications value, the probe **TNPI** was also applied for monitoring SO_2 derivatives in the mitochondria of living cells through the method of dual-channel ratio imaging.

2. Experimental section

2.1. Main instruments and reagents

All reagents are from commercial suppliers and no further purification was required. Column chromatography silica gel used in the experiment was 200–300 mesh. Melting points were measured by using a Gongyi X-5 microscopy digital melting point apparatus. IR spectra were recorded by using an Electrothemal Nicolet 380 spectrometer. The NMR spectra of ^1H and ^{13}C were measured on the AVANCE II spectrometer with tetramethylsilane (TMS) as the internal reference material. Bruker APEX IV spectrometer was used for high resolution mass spectrometry analysis (HRMS). UV–vis spectrum were obtained from T6 new century spectrometer. Model PHS-3C pH meter was used for pH measurement. Fluorescence spectra measurements were performed on the F-2700 fluorescence spectrophotometer. Olympus FV1000 laser-scanning confocal microscope was used for fluorescence imaging.

2.2. Procedure for spectral measurements

A solution of **TNPI** (1 mM) was prepared in DMF. Other testing analytes (KF, NaCl, KBr, KI, Na_2CO_3, $NaHCO_3$, $NaNO_3$, $NaNO_2$, AcONa, Na_2S, $NaHSO_3$, Na_2SO_3, Na_2SO_4, $Na_2S_2O_4$, $Na_2S_2O_5$, KSCN, $CaCl_2$, $MgCl_2$, $ZnCl_2$, Cys, Hcy, GSH, H_2O_2 and $NaClO_4$) were prepared as 10 mM aqueous solution with deionized water.

The stock solution of probe **TNPI** (100 μL) was added to a 10 ml of volumetric flask. Different amounts of analytes were added and diluted with PBS buffer (10 mM, pH 7.4) containing 5 % DMF to corresponding concentrations. Spectral acquisition time was 30 min.

2.3. Cell culture and fluorescence imaging

HeLa cells were incubated in medium (MEM, minimum essential medium, supplemented with 10 % fetal bovine serum at 37 °C, in 5 % CO_2). The cell suspension of 100 μL per well was then inoculated into a 96-well plate containing a cap slide and cultured overnight. Cells were treated with **TNPI**. Treated cells were further incubated for 24 h. 100 μL of CCK8 was added to each well and incubated at 37 °C for 30 min. The optical absorbance at 450 nm was measured.

The cultured HeLa cells were divided into four groups. The first group was incubated with 10 μM probe **TNPI** in PBS buffer (containing 0.5 % DMSO) for 30 min as a control group. The other three groups were incubated with different concentrations of sulfite (10 μM, 30 μM, 150 μM) in PBS buffer (containing 0.5 % DMSO) for 30 min, washed with PBS buffer solution for three times, and then incubated with 10 μM probe **TNPI** in PBS buffer (containing 0.5 % DMSO) for another 30 min. The cells were washed with PBS buffer solution 3 times before fluorescence imaging. The fluorescence images were obtained using Olympus FV1000 laser scanning microscope. The green light was excited at 405 nm and the emission spectrum was 500–550 nm. The red light is excited by an excitation light of 552 nm with an emission spectrum of 560–600 nm.

3. Results and discussion

3.1. Design and synthesis of *TNPI*

The pyrazoline moiety of the probe **TNPI** has been selected as a fluorophore due to its high quantum yield, low toxicity, and effective cell permeability [40–42]. Hemicyanine dye is a cationic dye that not only increases the water solubility of the probe **TNPI**, but also acts as an identification group of the SO_2 derivative. Moreover, hemicyanine cationic dyes can be easily absorbed by cell mitochondria, which makes the probe have a certain cell targeting property [34,43,44]. Thus, the combination of pyrazoline and hemicyanine moiety might be used to construct a mitochondria-targeted fluorescent probe with long wavelength emission for sensing SO_2 derivatives.

As shown in Scheme 1, addition of SO_2 derivatives interrupts the conjugation between pyrazoline and hemicyanine moieties based on the 1, 4-nucleophilic addition reaction in the vinyl group of **TNPI**. The synthesis of **TNPI** is illustrated in Scheme 2. The probe and intermediate structures were identified by ^1H NMR, ^{13}C NMR and/or HRMS spectra (see Supporting Information).

The synthesis of probe **TNPI** is shown in Scheme 2. Compound 1 can be obtained through previous literature reports [36].

1-(Naphthalen-2-yl)-3-phenylprop-2-en-1-one (2). To a solution of benzaldehyde (0.75 g, 7.05 mmol) in EtOH (10 mL) was added dropwise 5 mL of aqueous NaOH solution (4 mol/L) at 0 °C, and then was added 2-acetylnaphthalene (1.00 g, 5.88 mmol). The resulting mixture was stirred for 3 h at room temperature, filtrated. The residue was washed and recrystallized from EtOH to afford **2** as a yellow solid (1.38 g, 90.9 %). M.P. 163–165 °C; IR (film) υ_{max}: 3057.51, 1658.33, 1626.42, 1598.42, 1448.69, 1328.24, 1184.74, 1123.99, 760.88 cm^{-1}; ^1H NMR (400 MHz, DMSO-d_6): δ 8.96 (s, 1 H), 8.17 (d, J = 3.6 Hz, 1 H), 8.15 (d, J = 1.6 Hz, 1 H), 8.12–8.13 (m, 1 H), 8.05 (d, J = 8.4 Hz,1 H), 8.01 (d, J = 7.6 Hz, 1 H), 7.92–7.94 (m, 2 H), 7.83 (d, J = 15.6 Hz,4 H), 7.64–7.68 (m, 2 H), 7.47–7.49 (m, 3 H); ^{13}C NMR (100 MHz, DMSO-d_6): δ 189.4, 144.5, 135.6, 135.4, 135.3, 132.9, 131.2, 131.1, 130.2, 129.5, 129.2, 129.0, 128.3, 127.5, 124.7, 122.6; HRMS ($C_{19}H_{14}O$) *m/z*: calculated for $[M+H]^+$: 259.1117; Found $[M+H]^+$: 259.1127.

*3-(Naphthalen-2-yl)-1,5-diphenyl-4,5-dihydro-1H-pyrazole(**3**)*. A mixture of compound **2** (0.50 g, 1.94 mmol) and phenyl hydrazine (0.25 g, 2.32 mmol) in 10 mL of glacial acetic acid was stirred at 90 °C for 5 h, cooled to room temperature, and then collected the solids. The residue was recrystallized with EtOH to give **3** as pale yellow solid (0.51 g,

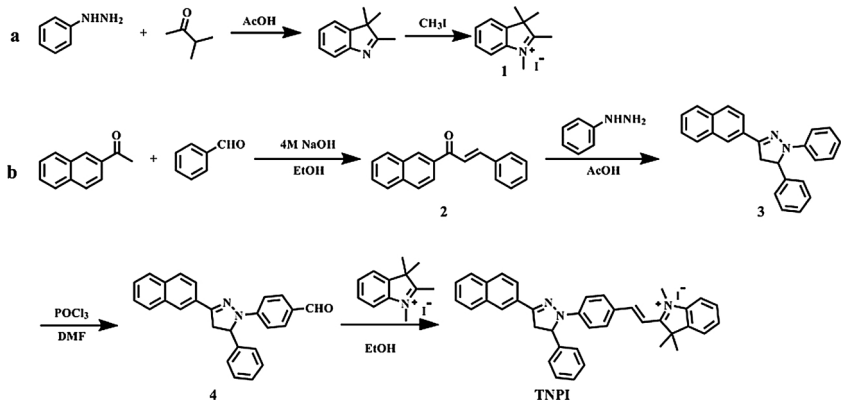

Scheme 2. Synthetic procedures of probe **TNPI**.

75.61 %). M.P. 187–189 °C; IR (film) υ_{max}: 2919.96, 1595.70, 1498.51, 1358.75, 1129.76, 827.95, 744.48, 692.29 cm^{-1}; ^1H NMR (400 MHz, $CDCl_3$): δ 8.18 (dd, J = 1.6, 8.4 Hz, 1 H), 7.79–7.86 (m, 4 H), 7.48 (d, J = 2.8 Hz, 1 H), 7.47 (d, J = 3.6 Hz,1 H), 7.36 (s, 2 H), 7.35 (d, J = 1.2 Hz, 2 H), 7.28–7.29 (m, 1 H), 7.19–7.23 (m, 2 H), 7.12–7.14 (m, 2 H), 6.81 (t, J = 6 Hz, 1 H), 5.33 (dd, J = 7.2, 12.4 Hz, 1 H), 3.95 (dd, J = 12.4, 17.2 Hz, 1 H), 3.27 (dd, J = 7.2, 17.2 Hz, 1 H); ^{13}C NMR (100 MHz, $CDCl_3$): δ 147.2, 145.2, 143.0, 133.80, 133.7, 130.8, 129.6, 129.4, 128.6, 128.5, 128.3, 128.0, 126.9, 126.8, 126.3, 125.5, 123.9, 119.6, 113.9, 65.0, 43.9; HRMS ($C_{25}H_{20}N_2$) m/z: calculated for $[M+H]^+$: 349.1699; Found $[M+H]^+$: 349.1713.

4-(3-(Naphthalen-2-yl)-5-phenyl-4,5-dihydro-1H-pyrazol-1-yl)benzaldehyde (4). $POCl_3$ (0.21 ml, 2.30 mmol) was added to 2 mL of DMF dropwise at room temperature. The mixture was stirred for 15 min at room temperature, added with compound 3 (0.40 g, 1.15 mmol, in 2 mL of DMF) at 0 °C, stirred at room temperature for 5 h, and poured into 10 mL of ice-water. The pH of the reaction mixture was adjusted to neutral with 30 % ammonia water. The reaction solution was extracted with ethyl acetate (3 × 20 mL). Organic layer was dried with anhydrous Na_2SO_4 and evaporated to dryness. The crude products were purified by silica gel column chromatography to give **4** as a yellow solid (0.35 g, yield: 81.7 %). M.P. 171–173 °C; IR (film) υ_{max}: 2924.10, 1681.10, 1592.74, 1519.15, 1406.13, 1222.99, 1162.57, 1129.21, 821.09, 700.20 cm^{-1}; ^1H NMR (400 MHz, $CDCl_3$): δ 9.78 (s, 1 H), 8.19 (dd, J = 1.6, 8.4 Hz, 1 H), 7.82–7.91 (m, 4 H), 7.72 (d, J = 8.8 Hz, 2 H), 7.49–7.55 (m, 2 H), 7.36–7.40 (m, 2 H), 7.28–7.33 (m, 3 H), 7.18 (d, J = 8.6 Hz, 2 H), 5.45 (dd, J = 5.6, 12 Hz, 1 H), 4.01 (dd, J = 12, 17.2 Hz, 1 H), 3.36 (dd, J = 5.6, 17.2 Hz, 1 H); ^{13}C NMR (100 MHz, $CDCl_3$): δ 190.7, 150.2, 148.6, 141.4, 133.9, 133.3, 131.8, 129.6, 129.6, 128.5, 128.4, 128.2, 128.0, 127.9, 127.0, 126.8, 126.2, 125.7, 123.5, 112.9, 63.6, 43.6; HRMS ($C_{26}H_{20}N_2O$) m/z: calculated for $[M+H]^+$: 377.1648; Found $[M+H]^+$: 377.1661.

*1,3,3-Trimethyl-2-(4-(3-(naphthalen-2-yl)-5-phenyl-4,5-dihy-dro-1H-pyrazol-1-yl)styryl)-3H-indol-1-Ium iodide (**TNPI**).* Compound **1** (0.08 g, 1.94 mmol) and compound **4** (0.10 g, 2.32 mmol) were dissolved in 5 mL of ethanol in a 25 mL of round bottom flask. The reaction mixture was stirred at 80 °C for 12 h. The solvent was then evaporated. The residue was purified by column chromatography using CH_2Cl_2/MeOH (v/v = 1:20) to give **TNPI** as a purple solid (0.11 g, yield: 63.9 %). M.P. 201–204 °C; IR (film) υ_{max}: 3361.55, 2924.10, 1569.60, 1516.22, 1402.81, 1291.68, 1170.67, 1113.84, 855.57, 708.72 cm^{-1}; ^1H NMR (400 MHz, $CDCl_3$): δ 8.29 (d, J = 16 Hz, 1 H), 8.18–8.21 (m, 2 H), 8.09 (d, J = 9.2 Hz, 2 H), 8.00 (d, J = 8.0 Hz, 1 H), 7.96–7.98 (m, 2 H), 7.79 (d, J = 8.0 Hz, 1 H), 7.75 (d, J = 8.0 Hz, 1 H), 7.56–7.59 (m, 3 H), 7.49–7.51 (m, 1 H), 7.36–7.40 (m, 2 H). 7.29–7.33 (m, 3 H), 7.21–7.29 (m, 3 H), 5.92 (dd, J = 4.4, 12 Hz, 1 H), 4.17 (dd, J = 12, 20 Hz, 1 H), 4.00 (s, 3 H), 3.43 (dd, J = 4.4, 18 Hz, 1 H), 1.74 (d, J = 4.4 Hz, 6 H); ^{13}C NMR (100 MHz, $CDCl_3$) δ 179.4, 154.4, 152.9, 148.5, 141.9, 141.4, 140.3, 134.4, 133.8, 132.8, 129.2, 129.0, 128.7, 128.2, 128.0, 127.6, 127.0, 126.7, 126.6, 125.4, 124.6, 123.2, 122.2, 113.9, 113.1, 105.9, 63.0, 51.1, 43.4, 35.4, 27.3; HRMS ($C_{38}H_{34}N_3I$) m/z: calculated for $[M-I]^+$: 532.2747; Found $[M-I]^+$: 532.2734.

3.2. Spectral changes of *TNPI* toward sulfite

The pH value is generally considered to be an important factor affecting the interaction between the substances. In order to obtain the influence of pH on the detection process, the fluorescence intensity of the probe **TNPI** solution was tested under different pH values (Fig.S1). The fluorescent intensity ratio of free probe **TNPI** (10 μM) was almost unchanged between pH 2 and pH 12. However, the solution of probe **TNPI** displayed a strong fluorescent intensity ratio enhancement in the presence of SO_3^{2-} over a wide pH range (5–9), which suggested that the probe can detect sulfite under physiological conditions. In order to get detection time of **TNPI** with sulfite, fluorescence kinetics experiments were carried out. As depicted Fig. 1, different concentrations of SO_3^{2-} were added to **TNPI** (10 μM). Although 200 μM SO_3^{2-} could complete the reaction with reaching an intensity plateau in 10 min, a low concentration of SO_3^{2-} took a longer time to achieve fluorescence intensity saturation. In addition, the fluorescence intensity ratio changes with time after adding lower concentrations of SO_3^{2-} were also investigated (Figure S2). Thus, 30 min after the addition of SO_3^{2-} was selected as the test time point in the experiments.

In order to investigate the selectivity, UV response experiments were carried out. The free probe **TNPI** (10 μM) showed a strong absorption peak at 558 nm (Fig. 2). However, after the addition of SO_3^{2-}, the maximum absorption was shifted to 380 nm. No similar spectral changes were observed in other analytes. Simultaneously, the color of

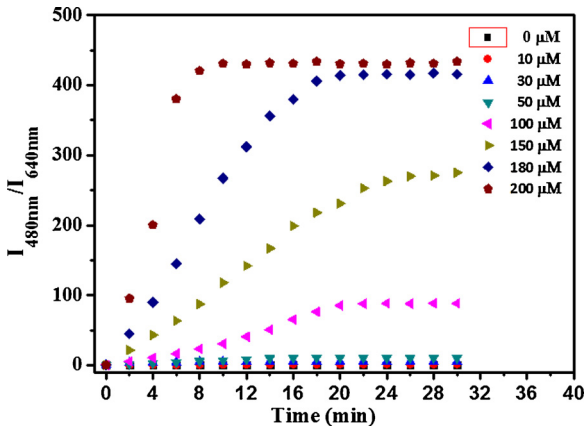

Fig. 1. Time-dependent fluorescence intensity ratio changes ($I_{480\ nm}/I_{640\ nm}$) of **TNPI** (10 μM) upon addition of varied concentrations of SO_3^{2-} in PBS buffer (10 mM, pH 7.4) containing 5 % DMF at room temperature.

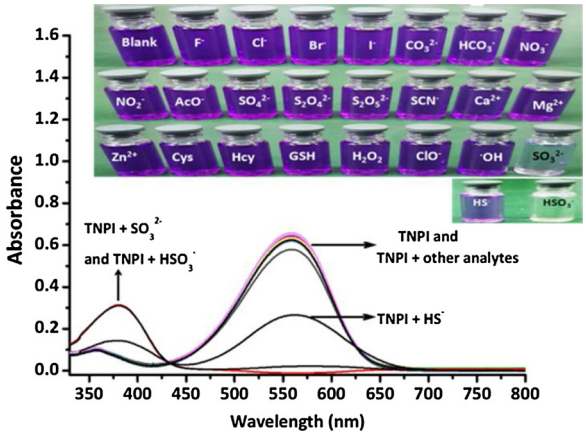

Fig. 2. Absorption spectra changes of the probe **TNPI** (10 μM) and the presence of 200 μM various analytes in PBS buffer (10 mM, pH 7.4) containing 5 % DMF as a co-solvent at room temperature. The color changes were shown in the inset.

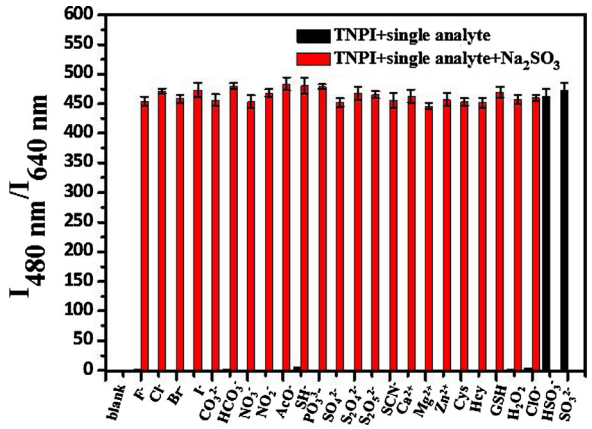

Fig. 4. Fluorescence response of probe **TNPI** (10 μM) toward SO_3^{2-} (200 μM) and other small biological species (200 μM) at fluorescence intensity ratios ($I_{480\ nm}/I_{640\ nm}$) in PBS buffer (10 mM, pH 7.4) containing 5 % DMF as a co-solvent at room temperature. The mixture was kept for 30 min before the fluorescence intensity was measured.

TNPI solution changed from purple to colorless, whereas no obvious changes were observed in other analytes (Fig. 2 inset). The selective change indicated that **TNPI** could act as a "naked eye" colorimetric indicator for sulfite detection.

The sensing behavior of probe **TNPI** toward various analytes was also tested with fluorescence spectroscopy in PBS buffer (10 mM, pH 7.4) containing 5 % DMF as a co-solvent, as shown in Fig. 3. The solution of free probe had an obvious red fluorescence at around 640 nm with excitation at 558 nm (fluorescence quantum yield: 0.13). Upon the addition of SO_3^{2-} and HSO_3-, the solution of **TNPI** showed a marked blue-green fluorescence with strong emission at 480 nm with excitation at 380 nm (fluorescence quantum yield of the product: 0.28), indicating the interruption of the π-conjugation between pyrazoline and hemicyanine moiety. This large emission shift (160 nm) resulted in the emission peaks being well distinguished before and after reacting with sulfite, and thus ratiometric sensing can be carried out, which provided a built in correction for biological environmental impacts. Only HS- led to a slight fluorescence change. The addition of other tested species induced negligible changes in the fluorescence intensity. The results demonstrated that **TNPI** showed a high selectivity toward SO_3^{2-}/HSO_3- over other analytes. SO_3^{2-} and HSO_3- showed the same fluorescent detection effect. Therefore, $SO_3^{2-}$was selected as the representative of SO_2 derivatives in the latter experiments. In order to detect the sulfite accurately, the sensing process of **TNPI** should not be interfered. Then, interference experiments were tested. SO_3^{2-} was added into to the solution of **TNPI** pretreated with a competing analyte. The results are shown in Fig. 4, all the relevant analytes measured have very little influence on sensing of SO_3^{2-}. In addition, lower concentration of SO_3^{2-} (30 μM) was tested in the presence of 200 μM competing analytes (Figure S3). We can see that even if the concentration of interfering analytes was much higher than SO_3^{2-}, SO_3^{2-} can also significantly increase the fluorescence ratio of the probe **TNPI** solution (10 μM). These results proved that **TNPI** had good anti-interference ability for sulfite recognition.

3.3. Quantitative responses of *TNPI* toward sulfite

To study the sensitivity of the probe **TNPI** to sulfite, fluorescence spectra were recorded by adding different amounts of SO_3^{2-} into the solution of **TNPI** (Fig. 5). The probe **TNPI** had a weak fluorescence in the absence of SO_3^{2-}. Upon addition of increasing concentrations of SO_3^{2-}, the solution of **TNPI** showed a gradual enhancement in the fluorescence emission bond at 480 nm. In contrast, the fluorescence intensity of solution gradually decreases at 640 nm. The fluorescence intensity ratio ($I_{480\ nm}/I_{640\ nm}$) increased from 0.45–445 after adding 20 equiv. of Na_2SO3. Furthermore, the fluorescence intensity ratios showed a good linear relationship with the concentration of SO_3^{2-} (0–30 μM) (Fig. 6). The detection limit of **TNPI** for SO_3^{2-} was calculated to be 80 nM based on 3σ/slope method (see ESI). It can be concluded that **TNPI** was a sensitive indicator for sulfite in aqueous media from these results.

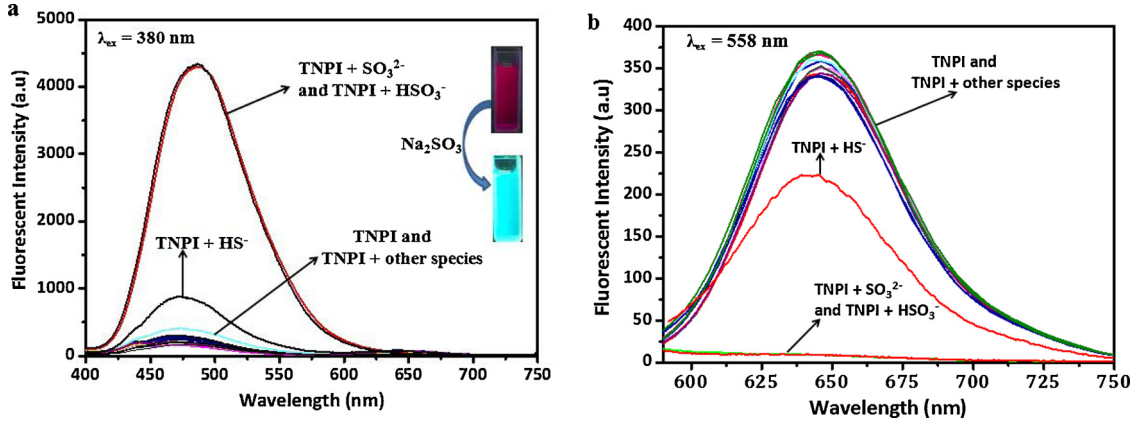

Fig. 3. Fluorescence spectra changes of the probe **TNPI** (10 μM) and the presence of 200 μM various analytes in PBS buffer (10 mM, pH 7.4) containing 5 % DMF as a co-solventat room temperature under excitation at 380 nm (a) and 558 nm (b).

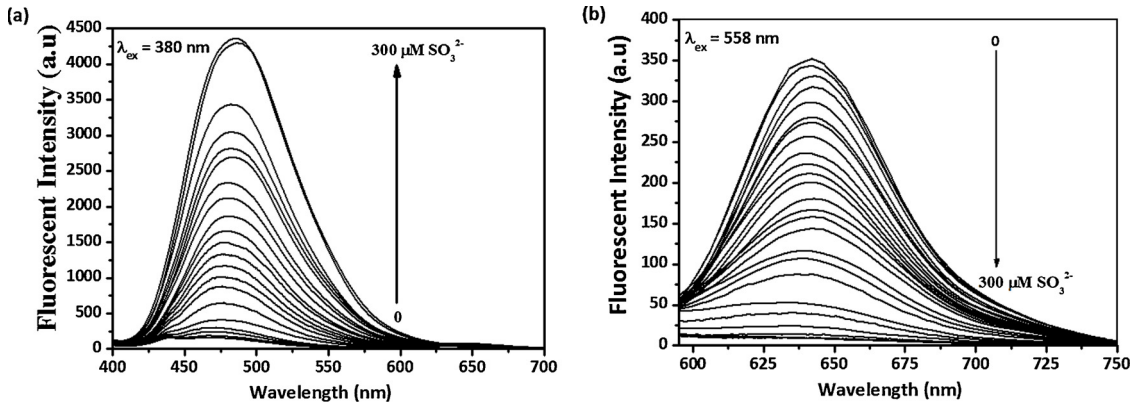

Fig. 5. The fluorescence spectra changes of probe **TNPI** (10 μM) with increasing amount of SO_3^{2-}. Each spectrum was obtained 30 min after SO_3^{2-} addition.

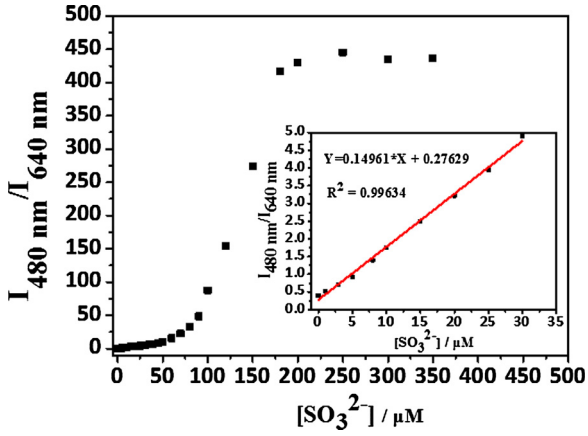

Fig. 6. Fluorescence intensity ratio changes ($I_{480\ nm}/I_{640\ nm}$) of probe **TNPI** (10 μM) against SO_3^{2-} concentrations from 0 μM–350 μM. Inset: The linear relationship between fluorescent intensity ratio and SO_3^{2-} concentration (0 − 30 μM).

3.4. The proposed sensing mechanism

In order to study the sensing mechanism, the Gaussian 09 program was firstly used for theoretical calculation [45]. As shown in Fig. 7, optimized molecular geometry of **TNPI** clearly showed π-conjugation between pyrazoline and hemicyanine moieties through a C═C double bond. This π-conjugation structure was corrupted in **TNPI-SO_3**, nucleophilic addition reaction product of C═C double bond of **TNPI** with SO_3^{2-}. We then further compared the highest occupied molecular orbital (HOMO) and lowest unoccupied molecular orbital (LUMO) of **TNPI** and **TNPI-SO_3** [71]. In **TNPI**, HOMO is mainly localized on the pyrazoline moiety with small distribution on hemicyanine, while LUMO is mainly localized on hemicyanine moiety. ICT from pyrazoline to hemicyanine moieties is clearly observed in this "D-π-A" structure. In **TNPI**-SO_3, HOMO is totally dominated by hemicyanine moiety and LUMO is dominated by pyrazoline moiety, respectively. The π-conjunction between pyrazoline and hemicyanine moieties is destroyed. Thus, the ICT process between the pyrazoline and hemicyanine of **TNPI-SO_3** is inhibited. Therefore, this could lead to a blue-shift in the absorption and emission spectra [46].

In order to understand the reaction mechanism of **TNPI** toward SO_3^{2-}, we verified the process of reaction by some tracking method.

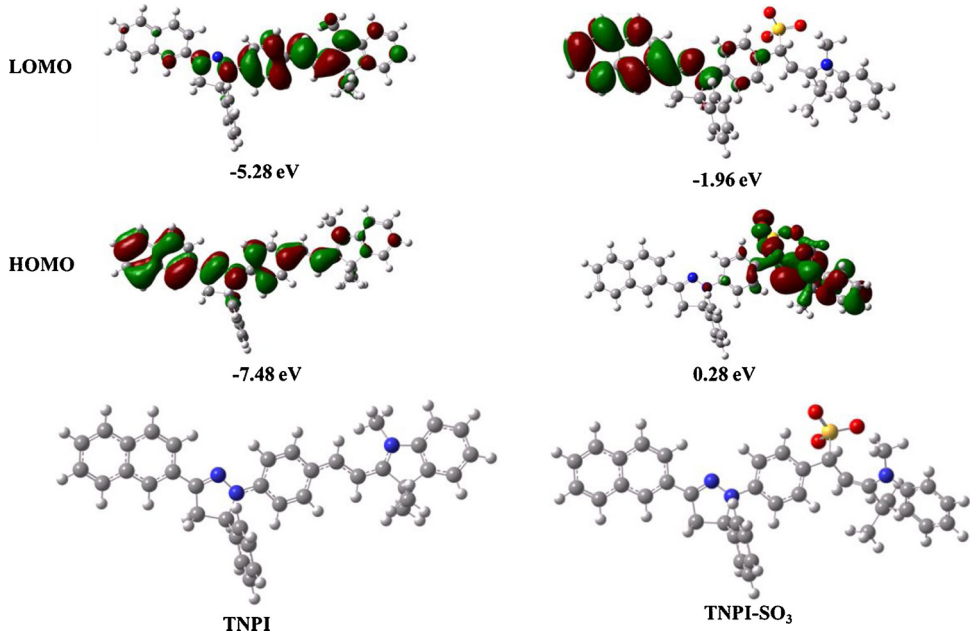

Fig. 7. Theoretical computation of **TNPI** and **TNPI-SO_3**. Optimized molecular geometries of **TNPI** and **TNPI-SO_3**, their HOMO and LUMO orbital distributions, and the corresponding electric energies.

Firstly, ^{1}H NMR titration was carefully performed (Fig. S4). An obvious difference was observed before and after the reaction of **TNPI** and SO_3^{2-}. Signals corresponding to the protons (7.79 ppm for Hb and 7.75 ppm for Ha) assigned to the double bond hydrogens in the probe **TNPI** disappeared and new signals emerged at 6.59 ppm (Hb,) and 6.51 ppm (Ha,) after the reaction with SO_3^{2-}. Moreover, the proton signal for methyl group (Hc) in the structure of **TNPI** changed from 4.00 ppm to 2.94 ppm. Secondly, the product of reaction was confirmed using HRMS, where a dominant peak at *m/z* value of 635.2218 corresponds to [**TNPI** + HSO_3- + Na]$^+$ (Fig. S5). These experimental results implied that the sensing mechanism involves the nucleophilic attack of SO_3^{2-} on the vinyl group of the probe **TNPI**, which are in good accordance with the reports in literature [44,47]. The structure of conjugation was interrupted, causing a blue-shift phenomenon in the emission wavelength (Scheme 1).

3.5. Cellular imaging

Based on the above excellent results, the bioimaging application of probe **TNPI** was further explored. To evaluate cytotoxicity of **TNPI**, we conducted CCK8 assay in HeLa cells. Compared with the control, the cells incubated with 10 μM **TNPI** for 24 h still maintained a survival rate of 92.3 % (Fig. S6), which clearly indicated that **TNPI** could be suitably applied to the cultured cells.

To demonstrate the abilities of the probe to enter cells and image SO_2 derivatives in living cells, we performed a separate emission window using a confocal microscope [21,48]. As shown in Fig. 8, after incubating HeLa cells with **TNPI**, strong fluorescence in the red channel could be readily observed and slight fluorescence was captured in the green channel. However, when Hela cells were pre-incubated with different concentrations of SO_3^{2-} (10 μM, 30 μM, 150 μM) for 30 min before incubating with 10 μM **TNPI** under the same conditions, the red fluorescence receded while the green fluorescence gradually increased. Therefore, the probe has the potential application in detecting the distribution and concentration of SO_2 derivatives in cells through the method of dual-channel ratio imaging.

After the SO_3^{2-} imaging in cells, the distribution of the probe at the subcellular level was determined by the co-localization experiments in Hela cells [49,50]. The cells were pretreated with 0.5 μM **TNPI** and subsequently 200 nM Mito-Tracker Green (or 200 nM Lyso-Tracker Green). As expected, the fluorescence of **TNPI** in red channel also overlapped exactly with that of Mito-Tracker Green in green channel (Pearson's correlation of 0.95) but not with that of lysosome (Fig. 9). The intensity profile of the red (**TNPI**) and green channels (Mito-Tracker Green) was almost identical from line profile. In order to preliminarily verify that the mitochondrial targeting of the probe **TNPI** was due to the cationic hemicyanine moiety, mitochondrial uncoupling agent 2,4-dinitrophenol (DNP) was used to eliminate the negative charge of the mitochondrial inner membrane of the cells. The result showed that the Pearson coefficient was significantly reduced (Figure S7). Therefore, the mitochondrial targeting of the probe **TNPI** may be due to the charge attraction between cationic hemicyanine moiety in the structure of probe **TNPI** with a positive charge and cellular mitochondrial membrane with the negative potential.

4. Conclusion

In summary, a novel red emission fluorescent probe (**TNPI**) has been developed for two-channel ratio detection of subcellular SO_2 derivatives. The probe exhibited not only outstanding sensitivity (80 nM) toward SO_2 derivatives but also high selectivity upon other species in a physiological pH aqueous solution. A large emission shift (160 nm) and a sharp emission ratio increase (from 0.45–445) were observed during the monitoring of SO_2 derivatives. The probe was also successfully used to monitor the changes of SO_2 derivatives in the mitochondria of cells through the formation of dual-channel ratio imaging. This probe would provide a promising chemical analysis tool for studying the application of SO_2 derivatives in medical diagnosis and disease research.

Author statement

Xiao-Bo Wang carried out the experiments and wrote the manuscript. Hui-Jing Li and Yan-Chao Wu designed experiments and revised the manuscript; Zhenxing Chi and Yun-Fei Cheng analyzed sequencing data and developed analysis tools; Xianshun Zeng directed the cell imaging experiments; Li-Juan Wang performed theoretical calculations.

Declaration of Competing Interest

The authors declare that they have no known competing financial interests or personal relationships that could have appeared to influence the work reported in this paper.

Acknowledgements

This work was supported by the Key Research and Development Program of Shandong Province (2019GSF108089), the Natural Science Foundation of Shandong Province (ZR2019MB009), the National

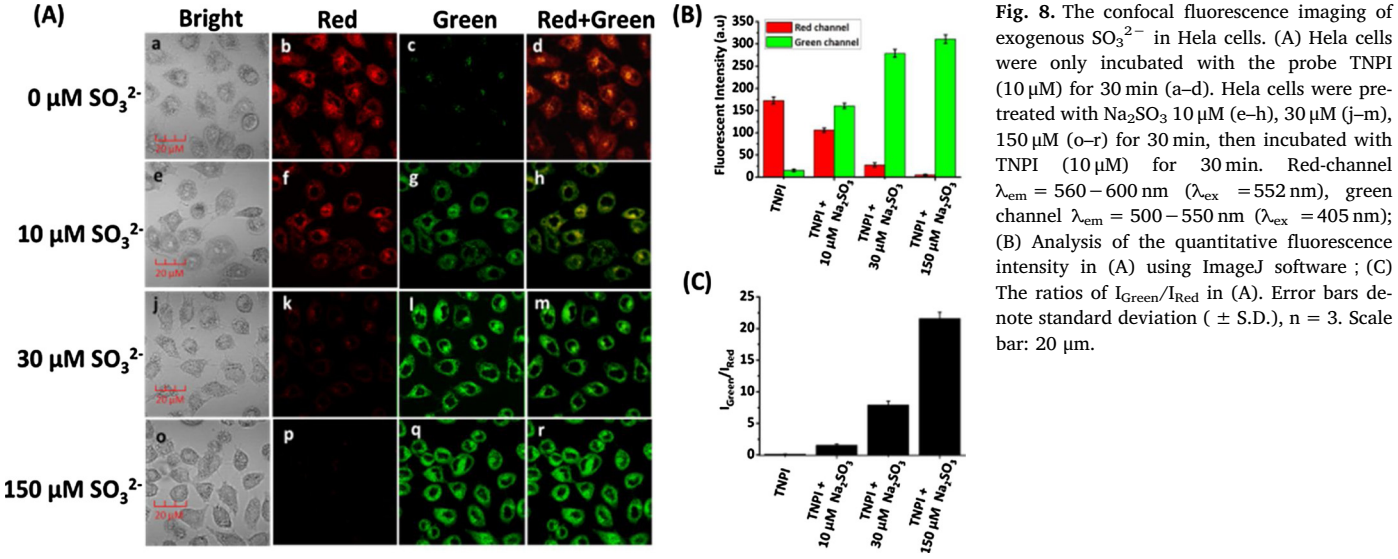

Fig. 8. The confocal fluorescence imaging of exogenous SO_3^{2-} in Hela cells. (A) Hela cells were only incubated with the probe TNPI (10 μM) for 30 min (a–d). Hela cells were pretreated with Na_2SO_3 10 μM (e–h), 30 μM (j–m), 150 μM (o–r) for 30 min, then incubated with TNPI (10 μM) for 30 min. Red-channel λ_{em} = 560 − 600 nm (λ_{ex} = 552 nm), green channel λ_{em} = 500 − 550 nm (λ_{ex} = 405 nm); (B) Analysis of the quantitative fluorescence intensity in (A) using ImageJ software ; (C) The ratios of I_{Green}/I_{Red} in (A). Error bars denote standard deviation (± S.D.), n = 3. Scale bar: 20 μm.

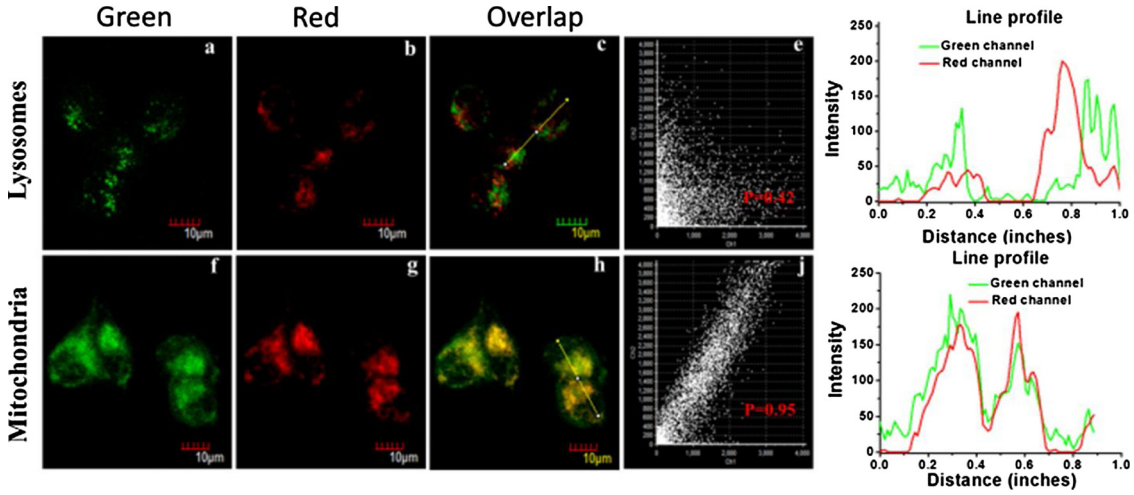

Fig. 9. Co-localization imaging in Hela cells. Cells were pretreated probe **TNPI** (5 μM, λ_{ex} = 552 nm, λ_{em} = 560 − 600 nm) for 30 min and then treated Mito-Tracker Green (200 nM, λ_{ex} = 488 nm, λ_{em} = 500 − 550 nm) and Lyso-tracker Green DND-26 (200 nM, λ_{ex} = 488 nm, λ_{em} = 500–550 nm) for 30 min. a and f represent green channel of commercial dye; b and g represent red channel of probe **TNPI**; c and h represent merged imaging between commercial dye and probe **TNPI**; e and j represent Pearson's correlation; Line profile: intensity profile of the yellow line in image overlap. Scale bar: 10 μm.

Natural Science Foundation of China (21672046, 21372054), and the Found from the Huancui District of Weihai City.

Appendix A. Supplementary data

Supplementary material related to this article can be found, in the online version, at doi:https://doi.org/10.1016/j.jphotochem.2019.112339.

References

[1] N. Sang, Y. Yun, H. Li, L. Hou, M. Han, G. Li, SO_2 inhalation contributes to the development and progression of ischemic stroke in the brain, Toxicol. Sci. 114 (2010) 226–236.
[2] J. Bai, P. Lei, J. Zhang, C. Zhao, R. Liang, Sulfite exposure-induced hepatocyte death is not associated with alterations in p53 protein expression, Toxicology 312 (2013) 142–148.
[3] F. Pannullo, D. Lee, L. Neal, M. Dalvi, P. Agnew, F.M. Connor, C. Sarran, Quantifying the impact of current and future concentrations of air pollutants on respiratory disease risk in England, Environ. Health 16 (2017) 29.
[4] A. Salurcan, M. Turkyilmaz, M. Ozkan, Effects of sulfur dioxide concentration on organic acids and β-carotene in dried apricots during storage, Food Chem. (2017) 412–421.
[5] S.C. Morgan, C.M. Scholl, N.L. Benson, M.L. Stone, D.M. Durall, Sulfur dioxide addition at crush alters saccharomyces cerevisiae strain composition in spontaneous fermentations at two canadian wineries, Int. J. Food Microbiol. 244 (2017) 96–102.
[6] R. Nassar, A. Trivella, S. Mokh, M. Al-Iskandarani, H. Budzinski, P. Mazellier, Photodegradation of sulfamethazine, sulfamethoxypiridazine, amitriptyline, and clomipramine drugs in aqueous media, J. Photochem. Photobiol. A: Chem. 336 (2017) 176–182.
[7] T.M. Chen, J. Gokhale, S. Shofer, W.G. Kuschner, Outdoor air pollution: nitrogen dioxide, sulfur dioxide, and carbon monoxide health effects, Am. J. Med. Sci. 333 (2007) 249–256.
[8] M. Kampa, E. Castanas, Human health effects of air pollution, Environ. Pollut. 151 (2007) 362–367.
[9] M.H. Stipanuk, I. Ueki, Dealing with methionine/homocysteine sulfur: cysteine metabolism to taurine and inorganic sulfur, J. Inherit. Metab. Dis. 34 (2011) 17–32.
[10] S.X. Du, H.F. Jin, D.F. Bu, X. Zhao, B. Geng, C.S. Tang, Endogenously generated sulfur dioxide and its vasorelaxant effect in rats, Acta Pharmacol. Sin. 29 (2008) 923–930.
[11] V.S. Lin, W. Chen, M. Xian, C.J. Chang, Chemical probes for molecular imaging and detection of hydrogen sulfide and reactive sulfur species in biological systems, Chem. Soc. Rev. 44 (2015) 4596–4618.
[12] B. Palenzuela, B.M. Simonet, A. Rios, M. Valcarcel, Determination of free and total sulphur dioxide in wine by use of an amalgamated piezoelectric sensor, Anal. Chim. Acta 535 (2005) 65–72.
[13] C.S. Pundir, R. Rawal, Determination of sulfite with emphasis on biosensing methods: a review, Anal. Bioanal. Chem. 405 (2013) 3049–3062.
[14] N. Altunay, R. Gurkan, A new simple UV-Vis spectrophotometric method for determination of sulfite species in vegetables and dried fruits using a preconcentration process, Anal. Methods 8 (2016) 342–352.
[15] H. Beitollahi, S. Tajik, P. Biparva, Electrochemical determination of sulfite and phenol using a carbon paste electrode modified with ionic liquids and graphene nanosheets: application to determination of sulfite and phenol in real samples, Measurement 56 (2014) 170–177.
[16] Y. Zhao, W. Qiu, C. Yang, J. Wang, Study on a novel oxidation process for removing arsenic from flue gas, Energ. Fuel 31 (2017) 693–698.
[17] J. Yin, Y. Hu, J. Yoon, Fluorescent probes and bioimaging: alkali metals, alkaline earth metals and pH, Chem. Soc. Rev. 44 (2015) 4619–4644.
[18] M.E. Moragues, R. Martínez-Máñeze, F. Sancenon, Chromogenic and fluorogenic chemosensors and reagents for anions, A comprehensive review of the year 2009, Chem. Soc. Rev. 40 (2011) 2593–2643.
[19] L. He, B. Dong, Y. Liu, W. Lin, Fluorescent chemosensors manipulated by dual/triple interplaying sensing mechanisms, Chem. Soc. Rev. 45 (2016) 6449–6461.
[20] W. Sun, S. Guo, C. Hu, J. Fan, X. Peng, Recent development of chemosensors based on cyanine platforms, Chem. Rev. 116 (2016) 7768–7817.
[21] Y. Ma, Y. Tang, Y. Zhao, S. Gao, W. Lin, Two-Photon and deep-red emission ratiometric fluorescent probe with a large emission shift and signal ratios for sulfur dioxide: ultrafast response and applications in living cells, brain tissues, and zebrafishes, Anal. Chem. 89 (2017) 9388–9393.
[22] K. Li, L.L. Li, Q. Zhou, K.K. Yu, J.S. Kim, X.Q. Yu, Reaction-based fluorescent probes for SO2 derivatives and their biological applications, Coord. Chem. Rev. 388 (2019) 310–333.
[23] D. Li, X. Han, Z. Yan, Y. Cui, J. Miao, B. Zhao, A far-red ratiometric fluorescent probe for SO_2 derivatives based on the ESIPT enhanced FRET platform with improved performance, Dye. Pigment. 151 (2018) 95–101.
[24] Y. Liu, J. Nie, J. Niu, W.S. Wang, W.Y. Lin, An AIE + ESIPT ratiometric fluorescent probe for monitoring sulfur dioxide with distinct ratiometric fluorescence signals in mammalian cells, mouse embryonic fibroblast and zebrafish, J. Mater. Chem. B Mater. Biol. Med. 6 (2018) 1973–1983.
[25] F. Chen, A. Liu, R. Ji, Z. Xu, J. Dong, Y. Ge, A FRET-based probe for detection of the endogenous SO_2 in cells, Dye. Pigment. 165 (2019) 212–216.
[26] H. Li, J. Fan, S. Long, J. Du, J. Wang, X. Peng, A fluorescent and colorimetric probe for imaging the mitochondrial sulfur dioxide in living cells, Sensor Actuat B-Chem 273 (2018) 899–905.
[27] Q. Wang, W.J. Wang, S.Q. Li, J. Jiang, D.X. Li, Y. Feng, H.T. Sheng, X.M. Meng, M.Z. Zhu, X. Wang, A mitochondria-targeted colorimetric and two-photon fluorescent probe for biological SO_2 derivatives in living cells, Dye. Pigment. 134 (2016) 297–305.
[28] D.P. Li, Z.Y. Wang, H. Su, J.Y. Miao, B.X. Zhao, Fluorescence detection of endogenous bisulfite in liver cancer cells using an effective ESIPT enhanced FRET platform, Chem. Commun. 53 (2017) 577–580.
[29] M. Zhao, D. Liu, L. Zhou, B. Wu, X. Tian, Q. Zhang, H. Zhou, J. Yang, J. Wu, Y. Tiana, Two water-soluble two-photon fluorescence probes for ratiometric imaging endogenous SO_2 derivatives in mitochondria, Sens. Actuators B Chem. 255 (2018) 1228–1237.
[30] Y.T. Yang, T.T. Zhou, B.Z. Bai, C.X. Yin, W.Z. Xu, W. Li, Design of mitochondria targeted colorimetric and ratiometric fluorescent probes for rapid detection of SO_2 derivatives in living cells, Spectrochim. Acta A. 196 (2018) 215–221.
[31] W. Gao, Y. Ma, W. Lin, A mitochondria-targeted and deep-red emission ratiometric fluorescent probe for real-time visualization of SO_2 in living cells, zebrafish and living mice, Analyst 144 (2019) 4972–4977.
[32] D.P. Li, Z.Y. Wang, J. Cui, X. Wang, J.Y. Miao, B.X. Zhao, A new fluorescent probe for colorimetric and ratiometric detection of sulfur dioxide derivatives in liver cancer cells, Sci. Rep. 7 (2017) 45294.
[33] D. Zhang, A. Liu, R. Ji, J. Dong, Y. Ge, A mitochondria-targeted and FRET-based ratiometric fluorescent probe for detection of SO_2 derivatives in water, Anal. Chim. Acta 1055 (2019) 133–139.

[34] G. Song, A. Liu, H. Jiang, R. Ji, J. Dong, Y. Ge, A FRET-based ratiometric fluorescent probe for detection of intrinsically generated SO_2 derivatives in mitochondria, Anal. Chim. Acta 1053 (2019) 148–154.
[35] F. Chen, A. Liu, R. Ji, Z. Xu, J. Dong, Y. Ge, A FRET-based probe for detection of the endogenous SO_2 in cells, Dye. Pigment. 165 (2019) 212–216.
[36] X. Kong, J. Yin, M. Li, L. Zhu, B. Dong, Y. Ma, W. Lin, Simultaneously imaging of SO_2 in lysosomes and mitochondria based on a dual organelle-targeted fluorescent probe, Sens. Actuators B Chem. 292 (2019) 80–87.
[37] W. Liu, D. Zhang, B. Ni, J. Li, H. Weng, Y. Ye, Mitochondria-targeted and FRET based ratiometric fluorescent probe for SO_2 and its cell imaging, Sens. Actuators B Chem. 292 (2019) 330–336.
[38] T. Niu, T. Yu, G. Yin, H. Chen, P. Yin, H. Li, A novel colorimetric and ratiometric fluorescent probe for sensing SO_2 derivatives and their bioimaging in living cells, Analyst 144 (2019) 1546–1554.
[39] L. Tang, P. He, X. Yan, J. Sun, K. Zhong, S. Hou, Y. Bian, A mitochondria-targetable fluorescent probe for ratiometric detection of SO_2 derivatives and its application in live cell imaging, Sens. Actuators B Chem. 247 (2017) 421–427.
[40] X. Dai, T. Zhang, Y. Liu, T. Yan, Y. Li, J. Miao, B. Zhao, A ratiometric fluorescent probe for cysteine and its application in living cells, Sens. Actuators B Chem. 207 (2015) 872–877.
[41] T. Uchacz, G. Jajko, A. Danel, P. Szlachcic, S. Zapotoczny, Pyrazoline-based colorimetric and fluorescent probe for detection of sulphite, New J. Chem. 43 (2) (2019) 874–883.
[42] S.Q. Wang, Q.H. Wu, H.Y. Wang, X.X. Zheng, S.L. Shen, Y.R. Zhang, B.X. Zhao, Novel pyrazoline-based fluorescent probe for detecting glutathione and its application in cells, Biosens. Bioelectron. 55 (2014) 386–390.
[43] S. Liu, G. Ge, W. Dong, X. Peng, F. Liu, S. Chen, S. Sun, A mitochondrial targeting fluorescent probe based on the covalently linked anti-inflammatory drug dexamethasone and Cy7, Sens. Actuators B Chem. 253 (2017) 1145–1151.
[44] Y. Yao, Q. Sun, Z. Chen, R. Huang, W. Zhang, J. Qian, A mitochondria-targeted near infrared ratiometric fluorescent probe for the detection of sulfite in aqueous and in living cells, Talanta 189 (2018) 429–436.
[45] M.J. Frisch, G.W. Trucks, H.B. Schlegel, G.E. Scuseria, M.A. Robb, J.R. Cheeseman, et al., GAUSSIAN 09 (Revision B.01), Gaussian, Inc., Wallingford CT. Pittsburgh, PA, 2010 Gaussian, Inc..
[46] F. Zhou, Y. Sultanbawa, H. Feng, Y.L. Wang, Q.T. Meng, Y. Wang, Z.Q. Zhang, R. Zhang, A new red-emitting fluorescence probe for rapid and effective visualisation of bisulfite in food samples and live animals, J. Agric. Food Chem. 67 (2019) 4375–4383.
[47] M.F. Huang, L.N. Chen, J.Y. Ning, W.L. Wu, X.D. He, B.X. Zhao, A new lipid droplets-targeted fluorescence probe for specific detection of SO_2 derivatives in living cells, Sens. Actuators B Chem. 261 (2018) 196–202.
[48] Y. Zhao, Y. Ma, W. Lin, A near-infrared and two-photon ratiometric fluorescent probe with a large Stokes shift for sulfur dioxide derivatives detection and its applications in vitro and in vivo, Sens. Actuators B Chem. 288 (2019) 519–526.
[49] D. Cheng, Y. Pan, L. Wang, Z. Zeng, L. Yuan, X. Zhang, Y. Chang, Selective visualization of the endogenous peroxynitrite in an inflamed mouse model by a mitochondria-targetable two-photon ratiometric fluorescent probe, J. Am. Chem. Soc. 139 (2017) 285–292.
[50] U. Tamima, M. Santra, C.W. Song, Y.J. Reo, K.H. Ahn, A benzopyronin-based two-photon fluorescent probe for ratiometric imaging of lysosomal bisulfite with complete spectral separation, Anal. Chem. 91 (2019) 10779–10785.